Journal of
Materials Chemistry B

RSC Publishing

PAPER

View Article Online
View Journal | View Issue

Cite this: *J. Mater. Chem. B*, 2013, **1**, 2072

Nano-p–n junction heterostructure TiO_2 nanobelts for the electrochemical detection of anticancer drug and biointeractions with cancer cells

Jingjie Cui,*[ab] Yakun Ge,[a] Shaowei Chen,[c] Hongshi Zhao,[d] Hong Liu,*[b] Zhen Huang,[e] Huaidong Jiang[b] and Jing Chen[f]

Received 10th October 2012
Accepted 11th February 2013

DOI: 10.1039/c3tb00227f

www.rsc.org/MaterialsB

Nano-p–n junction heterostructures based on TiO_2 nanobelts with enhanced (001) facets were produced by assembling p-type semiconductor NiO nanoparticles on n-type surface-coarsened TiO_2 nanobelt surfaces. The heterostructures were then used as the sensing electrode for the electrochemical detection of anticancer drugs O^6-benzylguanine (O^6BG) and lung cancer cells. O^6BG exhibited an irreversible diffusion-controlled electrochemical process with an oxidation peak clearly identified at +0.78 V. For lung cancer cells one oxidation peak was found at +1.1 V and two reduction peaks at +0.30, and +0.90 V. These voltammetric features disappeared when O^6BG was added to the lung cancer cells, which was ascribed to the structural changes of the cell membranes caused by the anticancer drug. These results suggested that nano-p–n junction heterostructures based on TiO_2 nanobelts might serve as promising candidates for biosensing applications of anticancer drugs and tumor cells that will be of significance in diagnostic medicine, cancer diagnosis and molecular biology research.

1 Introduction

Nanomaterials have attracted great interest in the fields of biomedical research and biosensing applications including disease diagnosis, and detection of cancer cells and anticancer drugs.[1–5] High sensitivity is a critical element in the selection and development of sensing nanomaterials. Among these, high-purity anatase TiO_2, with a high percentage of reactive {001} facets, is generally desired for (bio)sensing applications.[6] However, anatase TiO_2 is a semiconductor with a wide band gap (3.2 eV), and the band gap usually increases when the size of TiO_2 diminishes to the nano-regime,[7] which strongly impedes charge transfer due to its high resistance. To facilitate charge transfer, a p–n junction is normally formed by joining p-type and n-type semiconductor films together in close contact. In addition, it is well-known that low dimensional nanostructures including nanobelts exhibit efficient charge transport dynamics, a critical component in the function and integration of nano-scale devices.[8–10] To this end, the fabrication of nano-p–n junction heterostructures based on TiO_2 nanobelts represents one of the effective methods to enhance the (bio)sensing performance of TiO_2-based devices, as illustrated in the present study in the electrochemical detection of O^6-benzylguanine (O^6BG).

Lung tumors are solid tumors, one of the leading causes of cancer death worldwide.[11] The DNA repair protein, O^6-alkylguanine DNA alkyltransferase (AGT), is highly expressed in solid tumors, and confers tumor resistance to a variety of anticancer alkylating agents.[12] The AGT can be binded by O^6-benzylguanine (O^6BG) rapidly. O^6BG is a very effective inactivator of alkyltransferase.[13] O^6BG provides an equally effective treatment of cancers either alone or in combination with other anticancer drugs.[14] The antineoplastic drug O^6BG, as an important anticancer therapeutic agent, is usually used in clinical treatment and biochemical research. Until now, to the best of our knowledge, the electrochemical analysis of O^6BG and its effect on cancer cells has not yet been reported.

Recently, our studies showed that TiO_2 nanobelts can be used as active sensing materials to sense purine bases, and surface-coarsened TiO_2 nanobelts display high sensitivity and selectivity.[15,16] In the present study, nano-p–n junction heterostructures based on TiO_2 nanobelts were produced by assembling p-type semiconducting NiO nanoparticles on n-type surface-coarsened TiO_2 nanobelts. Lung cancer cells were chosen as target cells, and the electrochemical behaviors of

[a]College of Life Information Science & Instrument Engineering, Hangzhou Dianzi University, Hangzhou 310018, China. E-mail: cuijingjie@hdu.edu.cn

[b]State Key Laboratory of Crystal Materials, Center of Bio & Micro/nano Functional Materials, Shandong University, 27 Shandanan Road, Jinan, 250100, PR China. E-mail: hongliu@sdu.edu.cn

[c]Department of Chemistry and Biochemistry, University of California, 1156 High Street, Santa Cruz, California 95064, USA

[d]Stem Cell and Tissue engineering School of Medicine, Zhejiang University, Hangzhou, 310018, China

[e]Department of Chemistry, Georgia State University, Atlanta, Georgia, USA

[f]The Institute of Developmental and Regenerative Biology, Hangzhou Normal University, Hangzhou, 310036, China

O^6BG, lung cancer cells and the effect of O^6BG on lung cancer cells were sensitively detected by using the nano-p–n junction heterostructure TiO_2 nanobelts as the biological nano-sensing materials. The relevant mechanism was also discussed.

2 Experimental section

2.1 Materials

Titania P-25 (TiO_2, *ca.* 75% anatase and 25% rutile), sodium hydroxide (NaOH), hydrochloric acid (HCl), phosphoric acid (H_3PO_4), sulfuric acid (H_2SO_4) and nickel nitrate ($Ni(NO_3)_2 \cdot 6H_2O$) were purchased from Sinopharm Chemical Reagents Corporation Ltd. O^6-Benzylguanine (O^6BG) was obtained from Aladdin (Shanghai, China). Conductive adhesive was purchased from China Shenzhen Capiton Sci-Technology Co., Ltd. Ultrapurified (Millipore) water was used throughout this study. All reagents were of analytical grade.

2.2 Preparation of TiO_2 nanobelts and NiO–TiO_2 p–n junction heterostructures

Titanate nanobelts were synthesized by a hydrothermal process in a concentrated NaOH aqueous solution. Commercial titania powders (Degussa Co., P-25, a mixture of anatase and rutile in a ratio of 3 : 1) were used as the precursor. Briefly, 0.1 g of the P-25 precursor was mixed with 20 mL of a 10 M NaOH aqueous solution, followed by a hydrothermal treatment at 180 °C in a 25 mL Teflon-lined autoclave for 72 h. The treated powders were washed thoroughly with de-ionized water, followed by a filtration and drying process, affording sodium titanate nanobelts, which were then immersed in a 0.1 M HCl aqueous solution for 24 h and washed thoroughly with water to produce hydrogen titanate nanobelts. The hydrogen titanate nanobelts obtained were dispersed into 20 mL of 0.02 M H_2SO_4 aqueous solution under magnetic stirring for half an hour. The mixed solution was then transferred into a Teflon-lined stainless steel autoclave up to 80% of the total volume, heated at 100 °C for 12 h, and cooled to room temperature in air. The wet products were then thoroughly washed with deionized water and then dried at 70 °C to obtain surface-coarsened hydrogen titanate nanobelts ($H_2Ti_3O_7$). These nanobelts were divided into two portions. One part was thermally annealed at 600 °C for 2 h, leading to the formation of surface-coarsened TiO_2 nanobelts. The other part was dispersed into the $Ni(NO_3)_2 \cdot 6H_2O$ solution (Ti and Ni at a mole ratio of 9 : 5) and then soaked for 5 h. Subsequently, the soaked samples were carefully collected from solution and dried in an oven at 110 °C overnight. Finally, the dried samples were heat-treated at 600 °C for 2 h to obtain NiO–TiO_2 p–n junction heterostructures.

2.3 Structure characterization

X-ray powder diffraction (XRD) patterns were obtained on a Bruker D8 Advance powder X-ray diffractometer with Cu-Kα radiation (λ = 0.15406 nm). High resolution transmission electron microscope (HRTEM) images were obtained with a JEOL JEM 2100 microscope. All experiments were performed at room temperature.

2.4 Preparation of TiO_2 nanobelt-modified electrodes and electrochemical studies

2.4.1 Electrode preparation. A glassy carbon electrode (3 mm in diameter) was polished with 0.05 μm α-Al_2O_3 suspensions until a mirror surface was obtained, and rinsed extensively with anhydrous ethanol and de-ionized water. The electrode was then electrochemically cleaned in 0.5 M H_2SO_4 by cycling potentials between −0.3 and +1.8 V at 100 mV s^{-1} until a steady cyclic voltammogram was obtained. A conductive adhesive (CA) was drop-cast onto the cleaned glassy carbon electrode (GCE) surface, onto which 3 μL of an ethanolic suspension of TiO_2 nanobelts (0.5 mg mL^{-1}) was added in a dropwise fashion. After drying, the resulting electrodes were denoted as TiO_2/CA/GCE or p–n-NiO–TiO_2/CA/GCE.

2.4.2 Electrochemical investigation of anticancer drug O^6BG. Electrochemical measurements were performed in a three-electrode configuration. The TiO_2 nanobelt-modified electrodes prepared above were used as the working electrode. A Pt foil acted as the auxiliary electrode. All potentials were referenced to an Ag/AgCl/saturated KCl reference electrode. The sterilized phosphate buffer solution (PBS, 0.1 M, pH 7.4) was used as the electrolyte in all experiments. The electrochemical behavior of O^6BG was detected by using the TiO_2 nanobelt-modified electrodes. Voltammetric data were acquired with a CHI 660C electrochemical workstation.

2.4.3 *In situ* electrochemical investigation of cancer cells and anticancer drug effect. Lung cancer cells were cultured in a dish in a RPMI 1640 medium (GIBCO) supplemented with 10% fetal calf serum (SIJIQING) at 37 °C in a humidified atmosphere containing 5% CO_2. In electrochemical measurements, TiO_2 nanobelt-modified electrodes prepared above were used as the working electrode and directly immersed into the cell culture by slowly approaching the lung cancer cells, with the bottom of the culture dish just covered by a layer of lung cancer cells. The voltammetric response was acquired before and after O^6BG was added in a dropwise fashion. A Pt foil acted as the auxiliary electrode. All potentials were referred to an Ag/AgCl/KCl saturated reference electrode. Voltammetric data were acquired with a CHI 660C electrochemical workstation.

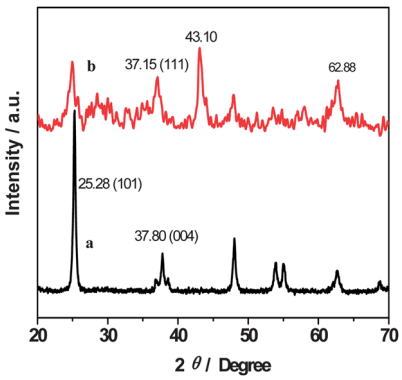

Fig. 1 X-ray diffraction (XRD) patterns of surface-coarsened TiO_2 nanobelts (a) without and (b) with the attachment of NiO nanoparticles.

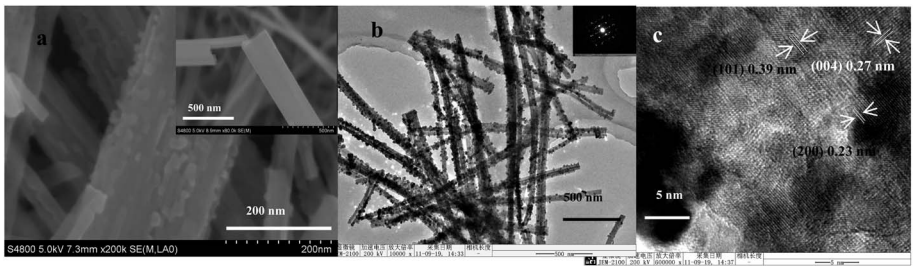

Fig. 2 Microstructure of nano-p–n junction heterostructure NiO–TiO_2 nanobelts: (a) TEM image and electron diffraction images (inset) and (b) HRTEM lattice fringes images.

3 Results and discussion

3.1 Structural characterizations

Analysis of the XRD patterns (Fig. 1a) of the surface-coarsened TiO_2 nanobelts confirms that these samples exhibited a rather pure anatase crystalline phase.[16] For the nano-p–n junction heterostructure NiO–TiO_2 nanobelts (Fig. 1b), in addition to the anatase TiO_2 features, the diffraction peaks at $2\theta = 37.15°$, 43.10°, and 62.88° can be indexed to the (111), (200) and (220) lattice planes of cubic NiO phase (JCPDS Card 78-429), respectively. From Fig. 1b, it can be seen that the (111) peak of NiO and the (004) peak of TiO_2 nanobelts overlap and the (101) peak of TiO_2 became much weaker and the ratio $I(004)/I(101)$ apparently increased after deposition of NiO, which facilitates the enhancement of (001) facets in the p–n-NiO–TiO_2 nanobelts, which will lead to high reactivity in the resulting nano-p–n junction heterostructure, as detailed below.[6,7,16]

Electron microscopy examination (Fig. 2) provides more information about the morphology and microstructure of the resulting nanobelts. Unmodified TiO_2 nanobelts[16] exhibit a width of 50 to 200 nm, length up to hundreds of micrometres, and a smooth surface (Fig. 2a, inset). In contrast, after an alkaline hydrothermal and acid etching process surface-coarsened TiO_2 nanobelts (Fig. 2a) were obtained.[15,16] To prepare nano-p–n junction heterostructures, NiO nanoparticles were assembled on the surface-coarsened TiO_2 nanobelts. From Fig. 2b, it can be seen that most NiO nanoparticles are tiny nanocrystals uniformly distributed on the outermost surface of the TiO_2 nanobelts, resulting in the formation of well-defined nano-p–n junction heterostructures on the TiO_2 nanobelt surface. The nanoparticle diameters can be estimated from the TEM image to be about 20 nm. The lattice fringes of the nano-p–n junction heterostructure NiO–TiO_2 nanobelts are easily identified from the HRTEM measurements (Fig. 2c), with a spacing of 0.39 nm, 0.27 nm and 0.23 nm, consistent with the $d101$, $d004$ spacing of anatase TiO_2 and the $d200$ spacing of cubic NiO, respectively. The anatase TiO_2 and cubic NiO crystallites can also be manifested in electron diffraction (ED) measurements, as highlighted in the inset of Fig. 2b.

3.2 Sensitive detection of anticancer drug O^6BG

The electrochemical activity of O^6BG was then investigated by using a glassy carbon electrode modified with the TiO_2 nanobelts prepared above. Fig. 3 shows the voltammograms of the TiO_2 nanobelt-modified electrodes (TiO_2/CA/GCE and p–n-NiO–TiO_2/CA/GCE) in 0.1 M PBS (pH 7.4) in the absence and presence of 0.1 mM O^6BG. From Fig. 3a, it can be seen that within the potential range of −0.9 to +1.8 V, an irreversible reduction peak appeared at about −0.5 V for both TiO_2 nanobelt-modified electrodes in 0.1 M PBS (pH 7.4) regardless of O^6BG, which may be ascribed to the electroreduction of Ti ions.[17]

Furthermore, one can see that the reduction peak becomes much stronger for the p–n-NiO–TiO_2/CA/GCE electrode. This may be explained by the formation of p–n junctions. For nano-p–n junction NiO–TiO_2 nanobelt heterostructures, an internal

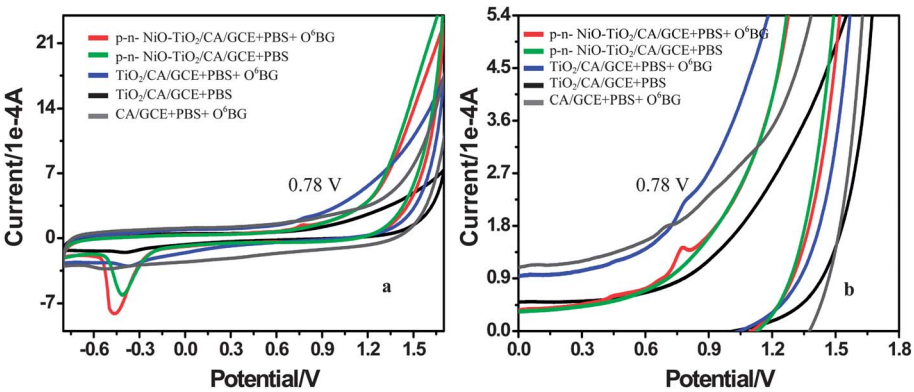

Fig. 3 Cyclic voltammetry (CV) curves for various modified electrodes in 0.1 M PBS (pH 7.4) without and with 0.1 mM O^6-benzylguanine (O^6BG). (b) The magnified cyclic voltammogram of the partial area in (a). Sweep rate, 100 mV s^{-1}.

field is generated at the interface of the NiO–TiO_2 nanobelts, where the p-type NiO regions are negatively charged and the n-type TiO_2 regions are positively charged. Therefore, the holes flow toward the negative side and the electrons flow toward the positive side. When the electrode potential was swept negatively, the electrons are biased toward the n-type TiO_2 regions by the internal field, and thus increasing the TiO_2 nanobelts' reduction current with the emergence of the enhanced electroreduction peak at −0.5 V for the p–n-NiO–TiO_2/CA/GCE electrode.

In addition, the control experiment in a blank PBS supporting electrolyte exhibited only a featureless voltammetric profile between +0.5 and +1.2 V (black and green curves in Fig. 3a and b), whereas irreversible oxidation peaks appeared at +0.78 V for the nanobelt electrodes in the presence of 0.1 mM O^6BG, which can be attributed to the electrooxidation of O^6BG (blue and red curves in Fig. 3a and b). Note that this peak potential was not observed at the CA/GCE electrode (gray curve in Fig. 3a and b). This indicates that the conductive adhesive (CA) did not affect the system of the resulting nanobelts electrodes when CA was used to fix nanobelts on the surface of GCE. From Fig. 3b, it can be seen that the voltammetric peak at p–n-NiO–TiO_2/CA/GCE in the presence of 0.1 mM O^6BG is much sharper and stronger than that at TiO_2/GCE, which suggests that the charge transfer kinetics and electroactivity were markedly enhanced by the assembly of nano-p–n junction heterostructure on the TiO_2 nanobelt surface. In response to the internal field, the holes flow toward the negative side (that is, the p-type NiO regions). When voltammetry sweep positively, the holes are biased toward the p-type NiO regions by the internal field. Then the holes are driven toward solution to electrooxide O^6BG by the electric field. It is known that holes are strong oxidants, thus facilitating the oxidation of O^6BG.

3.3 Kinetic characteristics of anticancer drug O^6BG at the p–n-NiO–TiO_2/CA/GCE electrode

Interestingly, the oxidation peak currents of O^6BG increase linearly with the square root of scan rates at the p–n-NiO–TiO_2/CA/GCE electrode, as depicted in Fig. 4a and b. This suggests that the oxidation of O^6BG was primarily controlled by diffusion, and charge transfer is rapid in the electrochemical process. This is consistent with the results in Section 3.2.

For an irreversible diffusion-controlled process, the relationship between the oxidation peak current (i_p) and diffusion coefficient D_0 is:[18]

$$i_p = 2.99 \times 10^5 n[(1-\alpha)n_\alpha]^{1/2} A C_0 D_0^{1/2} v^{1/2} \quad (1)$$

where v is the potential scan rate, C_0 is the reactant concentration in the bulk solution ($C_{O^6BG} = 1.0 \times 10^{-4}$ mol L^{-1}); A is the geometrical area of the working electrode ($A = 0.07$ cm^2); D_0 is the diffusion coefficient of the electroactive species in solution (cm^2 s^{-1}); n is the total number of electrons involved in the oxidation of O^6BG; n_α is the number of electrons involved in the rate-determining step and α is the electron transfer coefficient, which can be determined by the linear dependence of the oxidation peak potential ($E_{p,a}$) with the logarithm of the potential scan rate (v),[18,19]

$$E_{p,a} = E^o - RT/(1-\alpha)n_\alpha F[0.780 + \ln(D_0^{1/2}/k_s) + 1/2\ln(1-\alpha)n_\alpha F v/RT)] \quad (2)$$

where E^o is the formal potential; k_s is the standard rate constant of the surface reaction; R is the gas constant (8.314 J mol^{-1} K^{-1}); T is the absolute temperature ($T = 298$ K); F is the Faraday constant (96 485 C mol^{-1}). In the potential range examined, the plots of $E_{p,a}$ *versus* ln v were linear for the p–n-NiO–TiO_2/CA/GCE electrode, as manifested in Fig. 4c. Linear regressions show that for O^6BG oxidation at the p–n-NiO–TiO_2/CA/GCE electrode, $(1-\alpha)n_\alpha$ was estimated to be 0.696. For an irreversible process, the electron transfer coefficient (α) is usually thought of as 0.6, thus, n_α the number of electrons involved in the rate-determining may be estimated as 2. In addition, another approach was employed for the O^6BG oxidation reaction based on the difference between the peak potential E_p and the half-peak potential $E_{p/2}$ given by the equation:[18]

$$|E_p - E_{p/2}| = 47.7 \text{ mV}/(1-\alpha)n_\alpha \text{ (298 K)} \quad (3)$$

Thus, for an irreversible diffusion controlled process, $(1-\alpha)n_\alpha$ was estimated as 0.621, which is close to the value (0.696) from the slope of the plot 0.01843 obtained from Fig. 4c.

O^6BG, a guanine analogue with antineoplastic activity, exhibits apparent electrochemical activity most probably because of the guanine group. The total number of electrons involved in the oxidation of guanine is usually four.[20] Therefore,

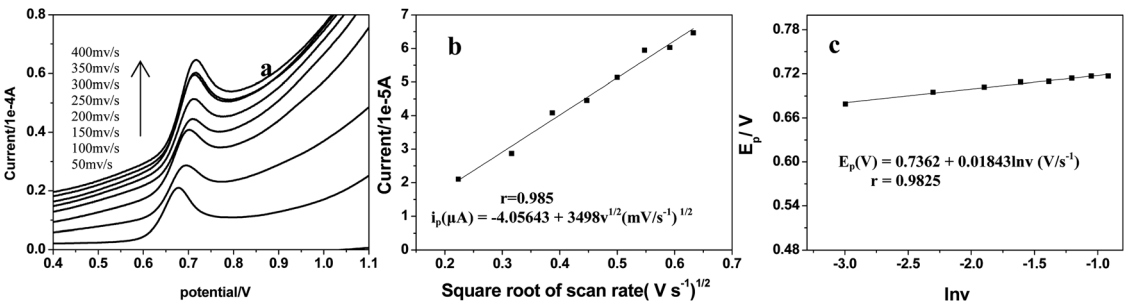

Fig. 4 Cyclic voltammograms at different scan rates (a); plot of peak current *vs.* the square root of scan rate (b); plot of E_p *vs.* ln v (c) for 0.1 mM O^6BG at the nano-p–n junction NiO–TiO_2 nanobelt heterostructures electrode in 0.1 M PBS (pH 7.4).

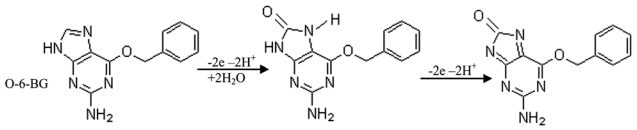

Scheme 1 The reaction mechanism of O^6BG.

in light of the above kinetic analysis, the oxidation of O^6BG at the p–n-NiO–TiO_2/CA/GCE electrode is likely to follow a two-step mechanism (Scheme 1), with the first two-electron oxidation as the rate-determining step. Based on eqn (1) and the slope of the i_p *vs.* $v^{1/2}$ plot in Fig. 4c, the D_0 value of O^6BG in the interface solution of the p–n-NiO–TiO_2/CA/GCE could be calculated to be about 2.083×10^{-7} cm^2 s^{-1}.

3.4 *In situ* electrochemical detection of cancer cells and anticancer drug effect

To examine the activity of O^6BG against lung cancer cells, lung cancer cells were cultured in a culture dish in a RPMI 1640 medium supplemented with 10% fetal calf serum at 37 °C in a humidified atmosphere containing 5% CO_2. The nano-p–n junction heterostructure sensitized TiO_2 nanobelts electrode was used to detect the biointeractions between lung cancer cells and anticancer drug O^6BG (Scheme 2). Fig. 5 shows the voltammograms of the lung cancer cells in the absence and presence of about 0.01 μM O^6BG. Within the potential range of 0 and +1.2 V, no obvious voltammetric features were observed in the absence of O^6BG at the electrode modified only with surface-coarsened TiO_2 nanobelts (Fig. 5a); in contrast, two reduction peaks and one oxidation peak appeared at +0.30, +0.90 V and +1.1 V at the electrode modified with the nano-p–n junction NiO–TiO_2 nanobelt heterostructures (Fig. 5b). These peaks may be ascribed to the electrochemical redox of the overexpressive membrane proteins (such as O^6-alkylguanine DNA alkyltransferase (AGT), P-glycoprotein (P-gp) and others) on the cellular surface.[21] Interestingly, these voltammetric peaks disappeared upon the addition of O^6BG (Fig. 5c). Note that tumor cells may release proteins and DNA into the extracellular environment, which causes the overexpression of these proteins.[22] Yet, the overexpressions can be significantly suppressed in the presence of O^6BG, as O^6BG can effectively inactivate AGT to inhibit the DNA replication of tumors, thereby killing the tumor cells and leading to the disappearance of the voltammetric peaks. During this process, the drugs caused the changes on the membrane of cancer cells due to their bonding interactions with the overexpressive membrane proteins (Scheme 3).[12] These results suggest that NiO nanoparticle–surface-coarsened TiO_2 nano-p–n junction nanobelt heterostructures may serve as promising active materials to detect biological processes relevant to cancer cells. Further work on the on-site electrochemical monitoring of physiological processes of cancer cells and the anticancer mechanism, and interfacial electron generation and the transport mechanism among cancer cells, anticancer drugs and nanobelts will be pursued in ongoing research.

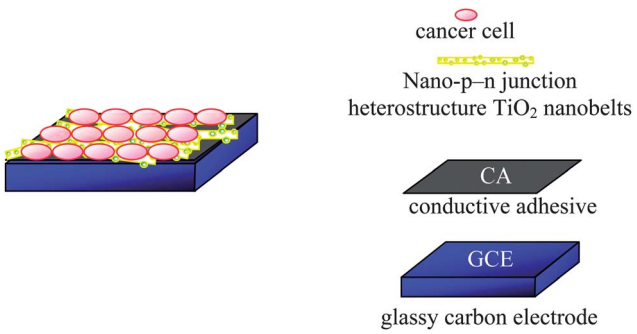

Scheme 2 Scheme for the illustration of the electrochemical detection of cancer cells based on functionalized the p–n-NiO–TiO_2/CA/GCE interface.

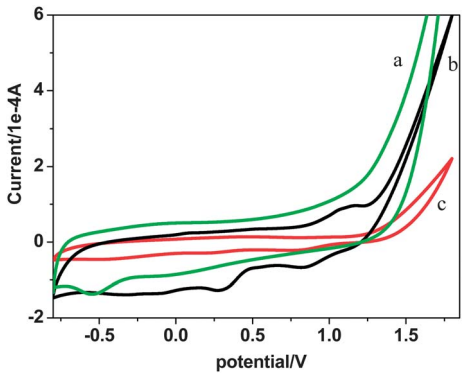

Fig. 5 Cyclic voltammetry (CV) behaviors for lung cancer cells at (a) the surface-coarsened TiO_2 nanobelts electrode and (b) the nano-p–n junction heterostructure NiO–TiO_2 nanobelt-modified electrode in a culture dish in a RPMI 1640 medium supplemented with 10% fetal calf serum; (c) the nano-p–n junction heterostructure NiO–TiO_2 nanobelt-modified electrode after about 0.01 μM O^6BG added to the above culture medium. Sweep rate, 100 mV s^{-1}.

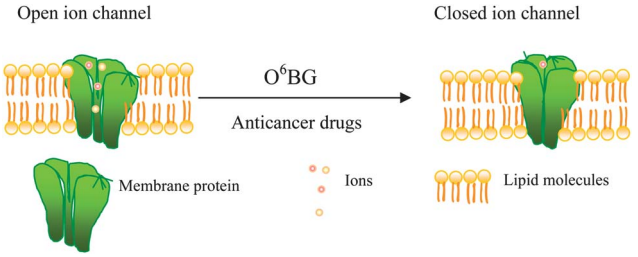

Scheme 3 Scheme for the illustration of the drugs caused the changes on the membrane of cancer cells.

4 Conclusion

In conclusion, nano-p–n junction heterostructure TiO_2 nanobelts have been produced by assembling p-type semiconductor NiO nanoparticles on n-type surface-coarsened TiO_2 nanobelts. The results of XRD and HRTEM show that the resulting sample consists of the cubic NiO phase and anatase phase with enhanced (001) facets and a quasi-one-dimensional nanostructure with roughened surfaces. The as-prepared NiO nanoparticle–surface-coarsened TiO_2 heterostructure nanobelts exhibited a markedly enhanced electrochemical activity and

sensitive detection of O^6BG, lung cancer cells and effect of O^6BG on lung cancer cells. The enhanced performance is ascribed to the nano-p–n junction heterostructure with enhanced (001) facets and the uniform distribution of the NiO nanoparticles on the TiO_2 nanobelt surface that effectively speedup charge transport and relieve polarization of the electrode. These results suggest that NiO nanoparticle–surface-coarsened TiO_2 nano-p–n junction heterostructure nanobelts may serve as promising active materials for biosensor applications of anticancer drugs and tumor cells that will be of significance to modern biochemical and biomedical research.

Acknowledgements

This research was supported by NSFC (NSFDYS: 50925205, Grant: 51102152, 51002089, 51172132), Independent Innovation Foundation of Shandong University (2010JQ004), China Postdoctoral Science Foundation (10000071311003) and Zhejiang Provincial Natural Science Foundation (Grant no. Y2110775).

References

1 P. P. Li, S. P. Liu, S. G. Yan, X. Q. Fan and Y. Q. He, *Colloids Surf., A*, 2011, **392**, 17.
2 Y. P. Luo, Y. Tian and Q. Rui, *Chem. Commun.*, 2009, 3014.
3 X. Yu, B. Munge, V. Patel, G. Jensen, A. Bhirde, J. D. Gong, S. N. Kim, J. Gillespie, J. S. Gutkind, F. Papadimitrakopoulos and J. F. Rusling, *J. Am. Chem. Soc.*, 2006, **128**, 11199.
4 R. Ovádeková, S. Jantová, S. Letašiová, I. Štepánek and J. Labuda, *Anal. Bioanal. Chem.*, 2006, **386**, 2055.
5 S. Chandra, N. Barola and D. Bahadur, *Chem. Commun.*, 2011, **47**, 11258.
6 H. G. Yang, C. H. Sun, S. Z. Qiao, J. Zou, G. Liu, S. C. Smith, H. M. Cheng and G. Q. Lu, *Nature*, 2008, **453**, 638.
7 X. B. Chen and S. S. Mao, *Chem. Rev.*, 2007, **107**, 2891.
8 U. Yogeswaran and S. M. Chen, *Sensors*, 2008, **8**, 290.
9 Z. L. Wang, *Annu. Rev. Phys. Chem.*, 2004, **55**, 159.
10 A. Noy, A. B. Artyukhin and N. Misra, *Mater. Today*, 2009, **12**, 22.
11 Y. Nagai, H. Miyazawa, Q. Hu, T. Tanaka, K. Udagawa, M. Kato, S. Fukuyama, A. Yokote, K. Kobayashi, M. Kanazawa and K. Hagiwara, *Cancer Res.*, 2005, **65**, 7276.
12 M. E. Dolan, R. C. Moschel and A. E. Pegg, *Proc. Natl. Acad. Sci. U. S. A.*, 1990, **87**, 5368.
13 M. E. Dolan, M. Y. Chae, A. E. Pegg, J. H. Mullen, H. S. Friedman and R. C. Moschel, *Cancer Res.*, 1997, **54**, 5123.
14 S. D. Konduri, J. Ticku, G. C. Bobustuc, R. M. Sutphin, J. Colon, B. Isley, K. K. Bhakat, S. S. Kalkunte and C. H. Baker, *Clin. Cancer Res.*, 2009, **15**, 6087.
15 J. J. Cui, D. H. Sun, S. W. Chen, W. J. Zhou, P. G. Hu, H. Liu and Z. Huang, *J. Mater. Chem.*, 2011, **21**, 10633.
16 J. J. Cui, D. H. Sun, W. J. Zhou, H. Liu, P. G. Hu, N. Ren, H. M. Qin, Z. Huang, J. J. Lin and H. Y. Ma, *Phys. Chem. Chem. Phys.*, 2011, **13**, 9232.
17 P. Tomčík, P. Jenčušová, M. Krajčíková, D. Bustin, A. Manová and M. Čakrt, *J. Electroanal. Chem.*, 2006, **593**, 167.
18 A. J. Bard and L. R. Faulkner, *Electrochemical Methods – Fundamentals and Applications*, John Wiley & Sons, New York, 2001, pp. 236–594.
19 E. Laviron, *J. Electroanal. Chem.*, 1974, **52**, 355.
20 N. de-los-Santos-Álvarez, P. de-los-Santos-Álvarez, M. J. Lobo-Castañón, R. López, A. J. Miranda-Ordieres and P. Tuñón-Blanco, *Electrochem. Commun.*, 2007, **9**, 1862.
21 F. He, Q. Shen, H. Jiang, J. Zhou, J. Cheng, D. D. Guo, Q. N. Li, X. M. Wang, D. G. Fu and B. A. Chen, *Talanta*, 2009, 77, 1009.
22 M. Esteller, M. Sanchez-Cespedes, R. Rosell, D. Sidransky, S. B. Baylin and J. G. Herman, *Cancer Res.*, 1999, **59**, 67.